ICONHIC2019
2nd International Conference on Natural Hazards & Infrastructure
23-26 June, 2019, Chania, Greece

# A numerical methodology for the fragility assessment of buried steel pipelines subjected to axial compression strains induced by seismic wave propagation

G. Tsinidis[1]
*University of Sannio, Italy & Vienna Consulting Engineers, Austria*

L. Di Sarno
*University of Liverpool, United Kingdom & University of Sannio, Italy*

A. Sextos
*University of Bristol, United Kingdom & Aristotle University of Thessaloniki, Greece*

P. Furtner
*Vienna Consulting Engineers, Austria*

## ABSTRACT

The paper presents a numerical methodology for the vulnerability assessment of buried steel natural gas (NG) pipelines, subjected to differential transient ground deformations, stemming from abrupt lateral site inhomogeneities. Idealized systems are considered, consisting of embedded steel NG pipelines crossing sites with vertical geotechnical discontinuity. The proposed analysis framework consists of two steps. A 3D trench-like continuum soil model, encasing a cylindrical shell model of the pipeline, is initially developed in ABAQUS, to compute the axial compressive response of the pipeline under an increasing level of axial relative ground deformation. The ground response under wave propagation is estimated by means of separate 1D nonlinear soil response analyses of the adjacent soil deposits, carried out in DEEPSOIL for an ensemble of selected ground seismic motions. The outcome of the soil response analyses, in terms of relative ground deformation patterns at pipeline's depth and peak ground velocity at the ground surface, is finally correlated with the predicted straining of the pipeline computed from the 3D analyses, in order to develop analytical fragility functions for predefined limit states, considering the associated uncertainties. The proposed approach, which is employed herein for an API-X65 buried gas pipeline with a diameter of 914.4 mm, offers high computational efficiency, whilst accounting for salient parameters that affect the axial response of steel NG pipelines.

*Keywords: steel NG pipelines, soil-seismic interaction, transient ground deformations, fragility curves*

## INTRODUCTION

The seismic risk assessment of buried pipelines is mainly performed by employing empirical fragility relations, constructed on the basis of observations of their response during past earthquakes (e.g. *ALA, 2001; NIBS, 2004*). A detailed review of available empirical relations may be found in *Tsinidis et al (2019a)*. However, a number of issues render the use of empirical fragility relations in the framework of quantitative risk assessment

[1] Corresponding Author: G. Tsinidis, *University of Sannio, Italy & Vienna Consulting Engineers, Austria,* tsinidis.grigorios@gmail.com

rather problematic. In particular, most of available relations refer to cast-iron or asbestos cement segmented pipelines, the seismic response of which is quite distinct compared to continuous pipelines, such as buried NG pipelines. Additionally, the implementation of *repair rate* as an engineering demand parameter, *EDP*, does not provide any information regarding the severity of damage, as well as the type of required repair. The most important drawback of empirical fragility relations is that they do not disaggregate between potential damage modes. Transient ground deformation may, under certain circumstances, trigger different damage modes on continuous buried NG pipelines, including (i) shell-mode or local buckling, (ii) beam-mode buckling, (iii) pure tensile rupture, (iv) flexural bending failure and (v) excessive ovaling deformation of the section (*O'Rourke MJ & Liu 1999*). The above distinct damage modes are associated with different risks and effects on the structural integrity and serviceability of the pipeline.

A limited number of analytical fragility curves that compute probabilities of failure for predefined limit states in the 'classical sense' have been proposed, recently (*Lee et al, 2016; Jahangiri & Shakib, 2018*). However, available analytical fragility functions refer to rather limited number soil-pipe configurations and do not cover NG pipelines with diameters larger than 800 mm that are commonly used in transmission NG networks. More importantly, the relevant numerical studies do not examine thoroughly salient parameters that may affect the response and hence the vulnerability of buried NG pipelines under seismically-induced transient ground deformations, such as the effects of soil heterogeneities along the axis of the pipeline, the internal operational pressure of the pipeline, the geometric imperfections of the walls of the pipes and the spatial variability of the seismic ground motion.

In the light of the above considerations and knowledge gaps, this paper presents an analysis framework for the development of analytical fragility curves for the structural assessment of buried steel NG pipelines subjected to axial compression caused by transient seismic ground deformations. The study focuses on pipelines crossing a vertical geotechnical discontinuity with an abrupt change on the soil properties, where the potential of high compression straining and hence buckling failures is expected to be increased under seismic transient ground deformations. The analytical framework is presented for API-X65 buried gas pipeline with a diameter of 914.4 mm. Crucial parameters namely the diameter, wall thickness, burial depth and internal pressure of the pipeline, the existence of wall imperfections of the pipeline, the trench backfill properties and compaction level, the pipe-trench interface friction characteristics and the soil deposits characteristics, are thoroughly accounted for. The analytical fragility curves are developed in terms of peak ground velocity at the ground surface, for four performance limit states, considering the associated uncertainties.

## ANALYTICAL FRAMEWORK

### Soil-pipe configurations

Fig.1 illustrates schematically the problem in hand. A continuous buried steel NG pipeline of external diameter, $D$, and wall thickness, $t$, is embedded in a surficial block of soil at a burial depth, $h$. The surficial block of soil is resting over a soil deposit with a vertical geotechnical discontinuity, which separates the deposit into *subdeposit 1* and *subdeposit 2*, with abrupt changes on their physical and mechanical properties. The total depth of the soil deposit is $H$. The soil-pipe system is subjected to vertically polarized plane shear seismic waves. The dissimilar ground movement ground movement of the adjusted soil subdeposits produces a differential horizontal ground deformation on the pipeline axis near the critical section of the geotechnical discontinuity, which subsequently is transferred via the pipe-trench backfill interface on the pipeline causing its axial straining. The analysis focuses on the compressive response of the pipe (more crucial one) and is carried out in steps, as discussed in the ensuing.

### Soil-pipe interaction analysis

A 3D trench-pipe numerical model is developed in ABAQUS (*ABAQUS, 2012*) to compute the axial compression response of the buried steel NG pipeline under an increasing level of seismically-induced relative axial ground displacement, $\delta_u$, considering the soil compliance. The axial ground displacement, $\delta_u$, is actually introduced in a quasi-static fashion, on the ground that the inertial soil-pipe interaction (SPI) effects are generally not important (*O'Rourke & Hmadi 1988*). Fig. 2 illustrates a model layout, with all relevant dimensions. The length of the 3D numerical model is aligned with the horizontal axis the pipeline presented in Fig. 1. Therefore, the relative ground deformation imposed on the pipeline by the dissimilar ground

movement of the adjusted soil subdeposits causes an in-plane axial deformation on the pipeline. The implementation of a 3D continuum model of the trench-pipe configuration allows for a rational simulation of localized buckling modes that might be developed in the pipe under high axial compression, as well as a rigorous simulation of the contact nonlinear phenomena, i.e. sliding and/or potential detachment in the normal direction between the pipeline wall and the surrounding ground.

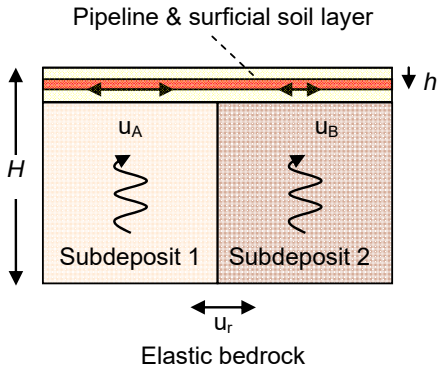


**Figure 1.** Schematic view of the examined problem (*h:* burial depth pf the pipeline, *H*: depth of the soil deposit, $u_r$: seismic displacement at bedrock, $u_A$ and $u_B$: horizontal seismic deformations of adjacent subdeposits)

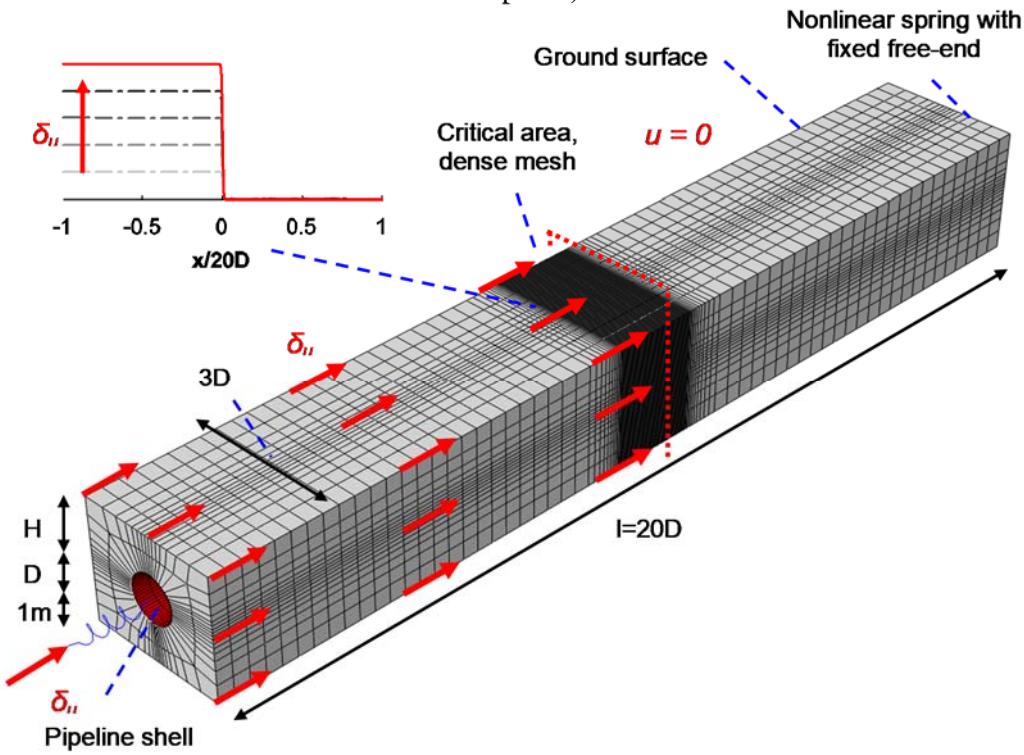


**Figure 2.** 3D trench-pipe numerical model for the computation of the axial compression response of the pipeline, under an increasing level of seismically-induced relative ground displacement, $\delta_u$

Linear hexahedral (brick-type) elements are used to model the trench backfill soil. In particular, average equivalent soil properties (i.e. average equivalent stiffness), corresponding to the strain-range that is anticipated for the selected ground seismic motions, are used to calibrate the elastic model used for trench backfill. These equivalent soil properties are evaluated via the 1D soil response analyses results, discussed in the following section. The pipeline is simulated by means of inelastic, reduced integration S4R shell elements, having both membrane and bending stiffness. The mesh density of the pipeline at the critical central section of the 3D numerical model, i.e. at the location of the geotechnical discontinuity where the axial strain of the pipeline is expected to maximize, is selected to be fine enough, i.e. around 1.0 – 2.0 cm, so as to resolve the inelastic buckling modes of an equivalent axially compressed unconstrained cylindrical steel shell (*Psyrras et al, 2019*). The mesh density away from the critical central zone is gradually decreased, in an effort to reduce the computation cost of the 3D analyses. The mesh discretization of the trench soil in the axial direction of the

model matches the exact mesh seed of the pipeline, so as to avoid any initial gaps during the generation of mesh. Nonlinear springs, acting parallel to the pipeline axis, are introduced at both sides of the pipeline, to reduce the required length of the 3D SPI model, whilst accounting for the effect of the infinite pipeline length on the axial response of the examined soil-pipe configurations. This simulation approach is inspired by *Vazouras et al (2015)* and is properly adjusted (i.e. the boundary conditions of the springs free nodes are properly selected) to account for the particular characteristics of the problem in hand (*Tsinidis et al, 2019b*). Typical static boundary conditions are applied at the bounding soil surfaces, while the ground surface is set free. The trench backfill-pipe interface is simulated by means of an advanced hard contact interaction model, available in *ABAQUS (2012).* The model allows for sliding and/or potential detachment in the normal direction between the interacting pipe and trench-soil elements. The shear behaviour of the interface model is controlled by the classical Coulomb friction model, through the introduction of a friction coefficient, $\mu$. The plastic behaviour of the steel pipelines is modelled through a classical flow plasticity model combined with a von Mises yield criterion, following *Psyrras et al (2019)*. In particular, Ramberg-Osgood curves, characterized by a yield offset equal to 0.5 %, are fitted to bilinear isotropic curves that describe the tensile uniaxial behaviour of the selected steel grade. Both 'perfect' pipelines and equivalent pipelines with initial geometric imperfections are examined. For the latter cases, a stress-free, biased axisymmetric imperfection is considered at the middle of the examined pipe and for a distance equal to 2.0 m. The imperfection is defined as a sinusoid modulated by a second sinusoid, resulting in a peak amplitude at the middle section of the length, where it is applied (*Psyrras et al, 2019*). The peak amplitude of the imperfection is set equal to 10 % of the pipe lining thickness. The exact same perturbation is introduced on the mesh of the trench soil, surrounding the pipeline, so as to prevent any initial gaps during the generation of the mesh that might affect the contact phenomena during loading.

The SPI analysis is carried out in steps as follows: the stress state caused by the gravity and the internal pressure of the pipeline is initially established, within a general static step, followed by a second step which aims at simulating the effect of transient ground deformation in quasi-static manner. In particular, during the second step the nodes of the one half of the trench model and the free node of the relevant nonlinear spring are fixed in the axial direction, i.e. $u = 0$, in the Fig. 2, whereas the nodes of the other half of the trench model and the free node of the relevant nonlinear spring are monotonically forced to move towards constraint part of the model, in a stepwise fashion, thus resulting in a relative axial displacement of the trench model equal to $\delta_u$. This displacement configuration is equivalent to the case where both halves of the trench model, are moving differently in the axial direction, causing the same differential ground movement $\delta_u$ on the examined system. The displacement pattern is kept constant with depth coordinate over the trench soil domain, for the sake of simplicity. The above kinematic loading induces shear stresses along the pipe-soil interface, which in addition to the axial loading induced by the adopted displacements of the free nodes of the springs result in an axial compression straining of the pipeline. The latter is traced for an increasing level of relative axial ground displacement, $\delta_u$, via a modified Riks solution algorithm, embedded in ABAQUS. The analysis results in a curve describing the relation between an increasing relative axial ground displacement, $\delta_u$, and the corresponding maximum compressive axial strain of the critical middle section of the pipeline. Since the response of the pipeline is computed for an increasing level of relative axial ground displacement, the outcome of one 3D SPI analysis may be used to examine the axial straining of the pipe under a variety of selected ground axial relative displacements, $\delta_{ue}$, caused by diverse seismic motions. Evidently, this is possible under implementation of mean equivalent soil properties for the trench- backfill soil, corresponding to the strain-range that is anticipated for the selected ground seismic motions.

**Soil response analysis under seismic wave propagation**

The response of selected soil deposits under seismic wave propagation is computed by means of 1D nonlinear soil response analyses of the adjacent subdeposits, carried out in DEEPSOIL (*Hashash et al, 2016*). Numerical models of the selected subdeposits presented in the following, are initially developed in the environment of the code, considering the surficial ground conditions and the elastic bedrock. The models are employed in a series of nonlinear time history analyses for the selected ensemble of seismic records. The hysteretic nonlinear response of the soil during ground shaking is considered in the analyses by means *G-γ-D* curves, which are properly selected for the examined deposits. Through the soil response analyses, time histories of the horizontal deformations of the soil columns are calculated at the burial depths of the pipelines, which are subsequently used to compute differential ground deformation patterns $\delta_{ue}$ for the selected pairs of adjusted sub-deposits. The latter are actually defined as follows: initially, the maximum of the maximum horizontal displacements of

the two columns, the relevant column, as well as the time step that this occurs, are all identified for each selected shaking motion. For this time step, the corresponding displacement of the adjacent column is then defined. Finally, $\delta_{ue}$ is evaluated as the difference between the above selected displacements of the columns. Additionally, time histories of the horizontal velocity are computed at the ground surface, which are used to evaluate the peak ground velocity PGV at ground surface. The latter is used as seismic intensity measure for the development of the analytical fragility curves.

**Combination of the results of the 3D SPI analyses with the predictions of the 1D soil response analyses**

The outcomes of the 3D SPI analyses and 1D soil response analyses are finally combined, to correlate the pipe response, in terms of maximum axial compression strain, $\varepsilon$, which is selected as engineering demand parameter, *EDP*, for the pipeline, with the ground response computed for each of the selected pairs of subdeposits and each ground motion. The latter combinations result in relationships of the *EPD* with the *PGV* at ground surface. The $\varepsilon$-*PGV* relationships are used to define analytical fragility curves for predefined performance limit states, considering all the associated uncertainties.

**Performance limit states & development of fragility functions**

Four performance limit states are defined on the basis of peak axial compressive strain $\varepsilon$ computed at the critical middle section, following *Jahangiri & Shakib (2018)*. The limit states, which are defined on the basis of relevant studies, guidelines, codes and regulations, refer to different return periods, ranging between 25 an 2475 years and are associated with different levels of damage on the pipeline (Table 1). For a more detailed presentation of the relevant definitions of the limit states the reader is referred to *Jahangiri & Shakib (2018).*

**Table 1.** Limit states adopted by Jahangiri & Shakib (2018), $t$ and $D$ are the thickness and diameter of pipe

| Limit state | Maximum limit strain (strain for examined pipe) | Description | Return period (years) |
|---|---|---|---|
| *Operable Limit State (OLS)* | $\varepsilon = \min(0.01, 0.4\times t/D)$ (0.0056) | Despite some minor plastic deformation, the pipeline will operate immediately after the event | 25 |
| *Pressure Integrity Limit State (PILS)* | $\varepsilon = \min(0.04, 1.76\times t/D)$ (0.0244) | Despite some significant deformations on the pipe, no leakage of containment is taken place | 95 |
| *Ultimate Limit State (ULS)* | $\varepsilon = \min(0.1, 4.4\times t/D)$ (0.0611) | A 'controllable' release of the containment of the pipeline is acceptable | 475 |
| *Global Collapse Limit State (GCLS)* | $\varepsilon = 0.15$ | A structural collapse is reported | 2475 |

Fragility functions describe the probability of exceeding different performance limit states, given a level of ground shaking. Following common approaches, the analytical fragility relations in this study are developed, employing a lognormal probability distribution function, as follows:

$$P\left(ds \geq ds \middle| S\right) = \Phi\left[\frac{1}{\beta_{tot}} \times \ln\left(\frac{PGV}{PGV_{mi}}\right)\right] \quad (1)$$

where $P\left(ds \geq ds \middle| S\right)$ is the probability of exceeding a particular limit state, *ds*, for a given seismic intensity level (defined by the peak ground velocity, *PGV*, at ground surface in this study), $\Phi$ is the standard cumulative probability function, $PGV_{mi}$ is the median threshold value of *IM*, required to cause the $i^{th}$ damage state, and $\beta_{tot}$ is the total lognormal standard deviation. Based on the above definitions, the analytical fragility curves may be sufficiently described by defining two main parameters, i.e. $PGV_{mi}$ and $\beta_{tot}$. $PGV_{mi}$ are defined on the basis of relevant regression analyses of the axial strain of the pipeline $\varepsilon$ with increasing *PGV* at ground surface, computed as described above. The lognormal standard deviation, $\beta_{tot}$, which describes the total variability associated with each fragility, is defined accounting for three primary sources of uncertainty (*NIBS, 2004*) namely the definition of damage states, $\beta_{ds}$, the capacity of the element, $\beta_C$, and the earthquake input motion (demand), $\beta_D$. The total uncertainty is estimated as the root of the sum of the squares of the component

dispersions. The uncertainty associated with the definition of damage states, $\beta_{ds}$, is set equal to 0.4, following HAZUS suggestions for buildings (*NIBS, 2004*). In a similar manner, the uncertainty due to the capacity, $\beta_C$, is assigned equal to 0.25. The last source of uncertainty, associated with the seismic demand, $\beta_D$, is described by the variability in response of the pipeline caused by the variability of ground motion, and it is calculated as the dispersion of the simulated damage indices with respect to the regression fit.

## CASE STUDIES

The analytical framework is employed in the case of an API 5L X65 steel pipeline ($\sigma_y$ = 448 MPa, $\sigma_u$ = 531 MPa) with the external diameter $D$ = 914.4 mm and wall thickness $t$ = 12.7 mm, i.e. a radius over thickness ratio $R/t$ equal to 36. The selected pipeline is designed for a maximum operational pressure of $p$ = 9 MPa, as per *ALA (2001)* regulations. The burial depth, $h$, of the selected pipeline, i.e. distance between the pipeline crown and ground surface, ranges between 1.0 m and 2.0 m, which constitute common burial depths for this infrastructure. The analyses are carried out for both 'perfect' pipelines and pipelines with initial geometric imperfection of the wall (i.e. $w/t$=0.1), pressurized to various internal pressures, i.e. $p$ = 0, 4 and 8 MPa, so that to cover a range of common operational pressures for this infrastructure. The pipeline is crossing a soil site of depth, $H$, equal to 30 m (Fig. 1). The site consists of a 3.0 m deep surficial layer of cohesionless material, resting upon pairs of subdeposits. An elastic bedrock with mass density, $\rho_b$ =2.2 t/m$^3$ shear wave velocity $V_{s,b}$ = 1000 m/s is assumed at the base of the site. Fig. 3 illustrates the gradients of the 'small strain' shear wave propagation velocities and the mass densities, $\rho$, of the selected cohesive and cohesionless subdeposits. The presented soil profiles are selected in pairs, in order to define subdeposits 1 and 2 in Fig. 1. In particular, three pairs are examined, i.e. Soil A - Soil B, Soil A - Soil C and Soil B - Soil C. Additionally, two different sets of mechanical and physical properties are examined for the surficial soil layer, corresponding to well or very well-compacted conditions (Table 2). This layer constitutes the trench backfill material for the examined pipelines and therefore is referred as either trench TA or trench TB in the ensuing, for the sake of simplicity. The shear moduli, $G$, presented in Table 2, correspond to 'average' equivalent soil stiffnesses, referring to the ground strain range anticipated for the selected seismic ground motions, and were estimated on the basis of 1D soil response analyses, discussed above. Relatively high values are adopted for the friction coefficient of the trench-pipe interface, $\mu$. The selected backfill compaction levels (upper bounds) as well as the 'rough' soil-pipe interfaces, are expected to lead to an increased pipeline axial straining under seismically-induced transient ground deformations. The nonlinear response of the selected soil deposits during ground seismic shaking is described by means of adequate $G$-$\gamma$-$D$ curves provided by Darendeli (2001), which are employed in the 1D soil response analyses carried out in DEEPSOIL.

An ensemble of 40 real ground motions is used in this study, which refer to earthquake moment magnitudes $M_w$, varying between 5 and 7.62, and were retrieved from the SHARE database (Giardini et al. 2013). The motions were recoded at epicentral distances, $R$, ranging between 3.4 and 71.4 km, on rock outcrop or very stiff soil, with shear wave velocity of first 30 m, $V_{s,30}$, ranging between 650 m/s and 2020 m/s. The input peak ground acceleration $PGA$ varies between 0.065 g to 0.91 g, while the peak ground velocity $PGV$ ranges between 0.031 m/s to 0.785 m/s.

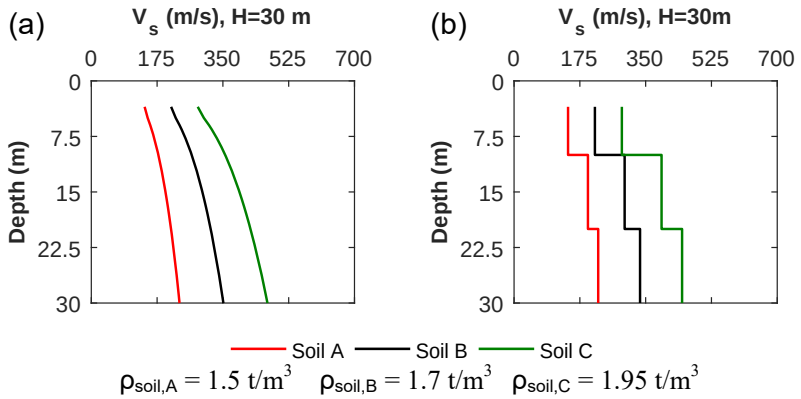


**Figure 3.** Shear wave velocity gradients of examined (a) cohesive and (b) cohesionless soil sub-deposits.

**Table 2.** Physical and mechanical properties of investigated surficial soils-trenches

| | Density, $\rho$ (t/m$^3$) | Poisson's ratio, $\nu$ | Shear modulus, $G$ (MPa) | Friction angle, $\varphi$ ($^o$) | Friction coefficient, $\mu$ |
|---|---|---|---|---|---|
| *Trench TA* | 1.65 | 0.3 | 37.1 | 35 | 0.45 |
| *Trench TB* | 1.9 | 0.3 | 63.15 | 44 | 0.78 |

## ANALYTICAL FRAGILITY CURVES

Having quantified the maximum strain for each limit state for the examined pipeline (Table 1), regression analyses of the natural logarithm of the computed peak axial strain $\varepsilon$ of the examined pipeline relative to the natural logarithm of the peak ground velocity $PGV$ at ground surface are carried out. The regressions are actually carried out for each soil-pipe configuration, by combining the numerical predictions of the analytical framework, referring to various levels of internal pressure for pipelines (i.e. $p$ = 0, 4 and 8 MPa) and various assumptions regarding the initial imperfection of the pipeline walls (i.e. combining the results referring to $w/t$ = 0 or $w/t$ = 0.1). The selection is made on the ground that the existence of wall imperfections is not a-priori known. Additionally, the use of results, referring to a range of internal pressures, allows for a general application of the provided fragility curves in networks with similar operational pressure characteristics. The results of the regression analyses are used to define the parameters that are required to construct the analytical fragility functions, i.e. $PGV_{mi}$ and $\beta_{tot}$. Table 3 summarizes these parameters for the examined cases.

**Table 3.** Median peak ground velocity corresponding to the limit states, $PGV_{m,i}$, and total lognormal standard deviation, $\beta_{tot}$, for the drawing of the analytical fragility curves ( - : the limit state is not reached).

| | | Cohesive soil deposit – Trench type TA | | | | | Cohesionless soil deposit – Trench type TA | | | | |
|---|---|---|---|---|---|---|---|---|---|---|---|
| **Soil** | ***h* (m)** | **$PGV_{m,OLS}$ (m/s)** | **$PGV_{m,PILS}$ (m/s)** | **$PGV_{m,ULS}$ (m/s)** | **$PGV_{m,GLS}$ (m/s)** | **$\beta_{tot}$** | **$PGV_{m,OLS}$ (m/s)** | **$PGV_{m,PILS}$ (m/s)** | **$PGV_{m,ULS}$ (m/s)** | **$PGV_{m,GLS}$ (m/s)** | **$\beta_{tot}$** |
| *A-B* | *1* | 0.922 | 3.101 | - | - | 0.807 | 1.042 | 3.716 | - | - | 0.779 |
| *A-B* | *2* | 1.286 | - | - | - | 0.720 | 2.073 | - | - | - | 0.556 |
| *A-C* | *1* | 1.203 | - | - | - | 0.755 | 1.011 | 3.740 | - | - | 0.763 |
| *A-C* | *2* | 1.832 | - | - | - | 0.625 | 1.268 | - | - | - | 0.745 |
| *B-C* | *1* | 2.974 | - | - | - | 0.702 | 4.900 | - | - | - | 0.697 |
| *B-C* | *2* | 4.159 | - | - | - | 0.655 | - | - | - | - | 0.646 |
| | | **Cohesive soil deposit – Trench type TB** | | | | | **Cohesionless soil deposit – Trench type TB** | | | | |
| **Soil** | ***h* (m)** | **$PGV_{m,OLS}$ (m/s)** | **$PGV_{m,PILS}$ (m/s)** | **$PGV_{m,ULS}$ (m/s)** | **$PGV_{m,GLS}$ (m/s)** | **$\beta_{tot}$** | **$PGV_{m,OLS}$ (m/s)** | **$PGV_{m,PILS}$ (m/s)** | **$PGV_{m,ULS}$ (m/s)** | **$PGV_{m,GLS}$ (m/s)** | **$\beta_{tot}$** |
| *A-B* | *1* | 0.401 | 0.900 | 1.484 | 2.424 | 1.101 | 0.427 | 0.983 | 1.646 | 2.728 | 1.110 |
| *A-B* | *2* | 0.409 | 0.946 | 1.589 | 2.641 | 1.166 | 0.427 | 1.004 | 1.702 | 2.856 | 1.178 |
| *A-C* | *1* | 0.374 | 0.836 | 1.373 | 2.235 | 1.138 | 0.383 | 0.852 | 1.397 | 2.269 | 1.144 |
| *A-C* | *2* | 0.384 | 0.885 | 1.483 | 2.460 | 1.210 | 0.392 | 0.911 | 1.536 | 2.563 | 1.197 |
| *B-C* | *1* | 0.927 | 2.959 | - | - | 0.894 | 1.200 | 4.450 | - | - | 0.838 |
| *B-C* | *2* | 0.962 | 3.222 | - | - | 0.907 | 1.385 | - | - | - | 0.798 |

Fig. 4 compares the analytical fragility relations developed within this study for 914.4 mm X65 pipelines embedded in the examined soil deposits at distinct burial depths, i.e. $h$ = 1.0 or 2.0 m. Evidently, a much higher fragility is observed for the pipeline when embedded in surficial soil-trench TB, compared to that reported for the equivalent pipeline embedded in surficial soil-trench TA. Actually, the ULS and GCLS limit states are not reached for the examined pipeline in trench TA. The higher shear stresses that are developed along the 'rougher' soil-pipe interface in case of surficial soil-trench TB result in an increased axial straining of the

pipeline, compared to the one predicted for the pipeline when embedded in trench TA. Additionally, the higher confinement that is offered by trench backfill TB on the pipeline, as a result of its higher compaction level and stiffness, partially reduces the upward bending of the pipeline during the kinematic loading of the system, which in turn leads to an increased localization of axial straining at the critical zone of the pipeline, near the geotechnical discontinuity (*Tsinidis et al, 2019b*). The above observations may explain increased fragility of the pipelines embedded in trench TB. It is worth noticing that the generally reduced fragility of the pipeline in surficial soil-trench TA (which may be seen as more common backfill condition in real networks) comes in line with the relatively good performance of buried NG pipelines reported during past earthquakes. Based on Table 1, the first two limit states constitute operational limit states, which do not lead to wall tearing and leakages and basically do not affect the flow of containment, at least not significantly. This makes the observation of relevant actual damages rather difficult, and may partially explain the reduced reported fragility of this infrastructure crossing similar sites, after actual earthquakes.

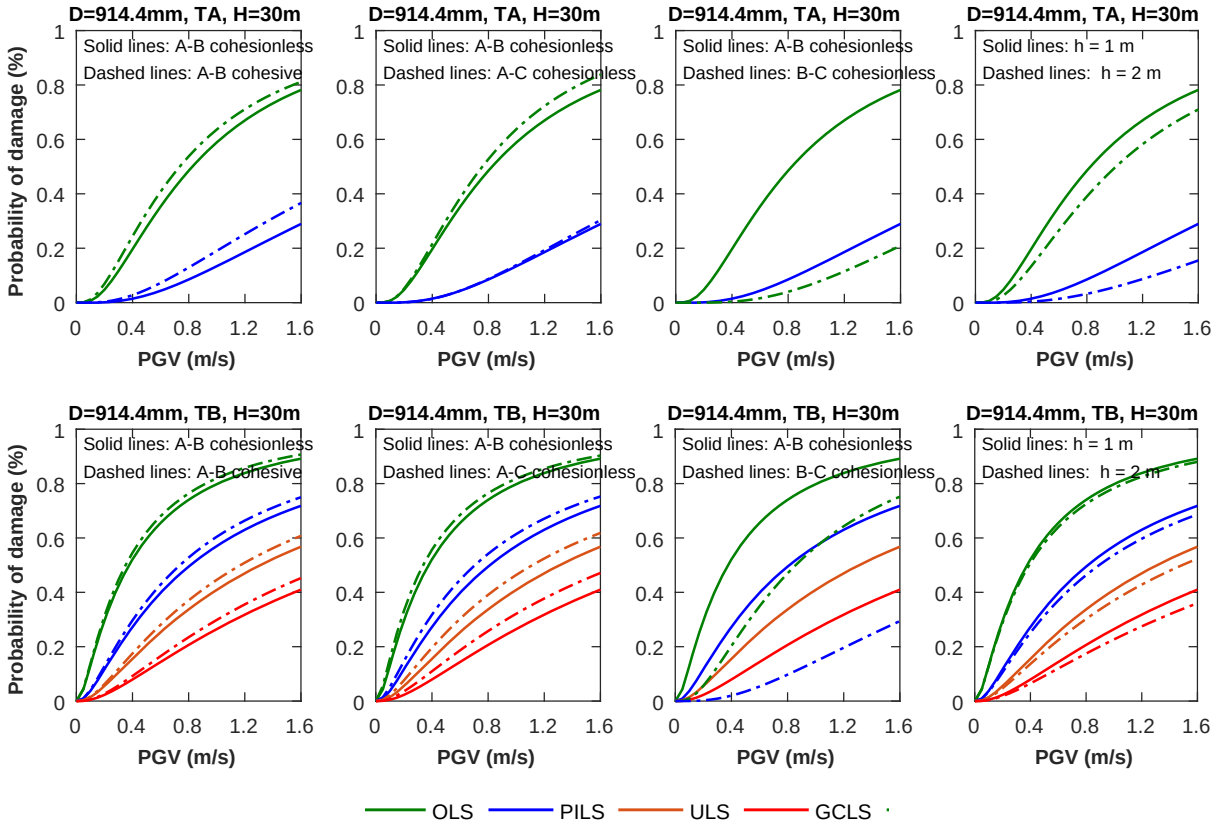


**Figure 4.** Comparisons of analytical fragility functions of API X65 914.4 mm pipelines, embedded in various soil deposits

The seismic fragility of the examined pipeline is found to be slightly lower when the pipeline is embedded in the site with cohesionless subdeposits, compared to the one computed for the site with the cohesive subdeposits (see subplots on the left-hand side of Fig. 4). The differences are attributed to the distinct ground response characteristics of the examined soil subdeposits, which induce different levels of axial straining on the embedded pipeline. Additionally, the higher contrast on the soil properties of the adjacent soil subdeposits, leads naturally to a more dissimilar response of the subdeposits, which induces higher straining on the pipeline, thus resulting to a higher damage potential for the pipeline. This hypothesis is verified by comparing the fragility curves developed for the pairs of subdeposits A-B and A-C. Indeed, a higher fragility is reported when the pipeline is embedded in site with subdeposits A-C (higher differences on the soil properties). Comparing the fragility of pipelines embedded in soils with subdeposits A-B and B-C, a much higher fragility is reported for the former soil site, even though the level of contrast of the properties of the adjacent subdeposits is the same for both cases. This is actually expected, given the 'lower' ground response of 'stiffer' soil deposits under ground shaking, i.e. the soil with subdeposits B-C in this case, as compared to soft soil deposits (i.e. soil with subdeposits A-B). In other words, the knowledge of the level of contrast of the properties of the adjacent subdeposits is not sufficed to clearly define the expected fragility of a buried pipeline for the examined kinematic loading condition. Finally, a higher fragility is systematically reported for pipeline, when embedded

at a burial depth, $h$ = 1.0 m, compared to the equivalent cases, where the pipeline is embedded deeper, i.e. $h$ = 2.0 m. This is attributed to the higher horizontal ground movement of the soil deposits towards the ground surface, under ground shaking, which causes higher relative ground deformations on the shallow-buried pipelines, hence increasing their axial response and damage potential.

## CONCLUSIONS

A numerical methodology for the vulnerability assessment of buried steel NG pipelines, subjected to differential transient ground deformations, stemming from abrupt lateral site inhomogeneities, was presented in this paper and applied on an API-X65 buried gas pipeline with a diameter of 914.4 mm, embedded in various soil deposits. The main conclusions of the study are summarized in the following:

- The seismic fragility of the examined pipeline against seismically-induced axial compression near geotechnical discontinuities was found to be rather reduced, when the pipeline was embedded in a medium-compacted backfill, with a 'relatively rough' trench-pipe interface being considered (i.e. surficial soil-trench TA in the present study). Actually for these conditions, the ULS and GCLS limit states, which are associated with major failures or collapse of the pipeline, were not reached for the examined pipe-soil configurations. This observation is in line with the reduced vulnerability of this infrastructure, reported during past earthquakes.
- On the contrary, a much higher fragility was reported for the pipeline, when embedded in a 'stiffer' very well compacted backfill, with a high friction coefficient $\mu$ being considered for the trench-pipe interface (i.e. surficial soil-trench TB). This was mainly attributed to the higher axial straining of the pipeline, which is caused by the higher stresses developed at the backfill-pipe interface during the ground displacement. Additionally, the higher confinement that is offered by the backfill on the pipeline reduces the bending of the pipeline towards the ground surface during the kinematic loading, thus increasing its local straining, finally contributing to an increased damage potential. It is worth noticing that the selected properties for surficial soil-trench TB may be considered as an upper bound for real conditions.
- Regardless of the backfill properties and soil-pipe interface characteristics, the fragility of pipelines was found to increase with increasing contrast of the soil properties of the adjacent soil subdeposits. Moreover, it was observed that the knowledge of the level of contrast of the properties of the adjacent subdeposits is not sufficed to clearly define the expected fragility of a buried NG pipeline under the examined seismic hazard, since the actual properties of the adjacent subdeposits affect considerably the ground response and hence the pipeline response and vulnerability.`
- A higher fragility was systematically reported for pipeline, when embedded at a burial depth, $h$ = 1.0 m, compared to the cases, where the equivalent pipeline was embedded at $h$ = 2.0 m.

Inevitably, there are some limitations of the analytical framework used herein. The effects of inertial SPI and of the evolution of stresses and deformations on the pipeline response, as well as time-dependent phenomena, such as fatigue and steel strength and stiffness degradation due to cyclic loading, are all neglected. Moreover, complex 2D wave phenomena near the geotechnical discontinuity are not being thoroughly investigated. However, the study covers a wide range of salient parameters that may affect the response and vulnerability of buried steel NG pipelines, crossing similar sites. In this context, the use of the analytical framework and analytical fragility curves may contribute towards a reliable quantitative risk assessment of, subjected to seismically-induced transient ground deformations.

## ACKNOWLEDGEMENTS

This work was supported by the Horizon 2020 Programme of the European Commission under the MSCA-RISE-2015-691213-EXCHANGE-Risk grant (Experimental and Computational Hybrid Assessment of NG Pipelines Exposed to Seismic Hazard, www.exchange-risk.eu). This support is gratefully acknowledged.

## REFERENCES

ABAQUS (2012). ABAQUS: theory and analysis user's manual version 6.12. Dassault Systemes Simulia. USA.

American Lifelines Alliance (ALA). (2001). Seismic fragility formulations for water systems. Part 1- Guidelines. ASCE-FEMA, Washington, DC, USA.

El Hmadi K., O'Rourke M. (1988). Soil springs for buried pipeline axial motion. Journal of Geotechnical Engineering, 114(11), pp. 1335-1339.

Giardini et al (2013) Seismic Hazard Harmonization in Europe (SHARE): Online Data Resource, doi: 10.12686/SED-00000001-SHARE

Hashash YMA, Musgrove MI, Harmon JA, Groholski DR, Phillips CA, Park D. (2016). DEEPSOIL 6.1, User Manual. USA.

Jahangiri V, Shakib H. (2018). Seismic risk assessment of buried steel gas pipelines under seismic wave propagation based on fragility analysis. Bulletin of Earthquake Engineering, 16(3), pp. 1571-1605.

Lee DH, Kim BH, Jeong SH, Jeon JS, Lee TH. (2016). Seismic fragility analysis of a buried gas pipeline based on nonlinear time-history analysis. International Journal of Steel Structures, 16(1), pp.231-242.

National Institute of Building Science (NIBS) (2004) Earthquake loss estimation methodology. HAZUS technical manual, Federal Emergency Management Agency (FEMA), Washington, USA.

O'Rourke MJ & Hmadi K (1988) Analysis of continuous buried pipelines for seismic wave effects. Earthquake Engineering and Structural Dynamics, 16, pp. 917-929.

O'Rourke MJ & Liu X. (1999). Response of buried pipelines subjected to earthquake effects. University of Buffalo, USA.

Psyrras N, Kwon O, Gerasimidis S, Sextos A (2019). Can a buried gas pipeline experience local buckling during earthquake ground shaking? Soil Dynamics and Earthquake Engineering, 116, pp. 511-529.

Tsinidis G, Di Sarno L, Sextos A, Furtner P (2019a). A critical review on the vulnerability assessment of natural gas pipelines subjected to seismic wave propagation. Part 1: Fragility relations and implemented seismic intensity measures. Tunnelling and Underground Space Technology, 86, pp. 279-296.

Tsinidis G, Di Sarno L, Sextos A, Furtner P (2019b).A critical review on the vulnerability assessment of natural gas pipelines subjected to seismic wave propagation. Part 2: Analytical methods. Tunnelling and Underground Space Technology (under review).

Vazouras P, Dakoulas P, Karamanos SA. (2015). Pipe-soil interaction and pipeline performance under strike-slip fault movements. Soil Dynamics and Earthquake Engineering, 72, pp. 48-65.